

# SPATIAL AVERAGING APPLICATIONS FOR THE TURBULENT FLOW OVER CANOPY MODELS

**Luciano Gonçalves Noletto**

lucianonoleto@unb.br

**Antonio C. P. Brasil Junior**

brasiljr@unb.br

Universidade de Brasília. Departamento de Engenharia Mecânica, LEA - Laboratório de Energia e Ambiente. 70910-900 Brasília. DF. Brazil.

**Abstract.** *The objective of this paper is to study the spatial average and its applications for the turbulent flow over a canopy model made of a set of several cylinders. Those cylinders are displaced in tandem arrangement. The simulation was conducted with Unsteady Reynolds Averaged Navier-Stokes (URANS) and the ANSYS CFX commercial software. Several horizontal planes were displaced at the end of the matrix, where the canopy boundary layer flow is fully developed. At those planes, a spatial averaging procedure will be applied, and with the average, the fluctuation will also be calculated. Therefore, a dispersive percentage will be calculated in order to see how far off the average the fluctuation is. This analysis will allow a study of the dispersive fluxes, as well as a flow threshold that will determine probing conditions for flow quantities.*

**Keywords:** *URANS, Canopy flow, Spatial Averaging, dispersive percentage*

## 1. INTRODUCTION

The study of canopy flows surpasses the field of turbulence. Its effects on forests and cities is a object of study not only in engineering and applied physics, but for meteorological purposes, agriculture, fire spread in forests, pollutant dispersion, biology and hydrology. The gas and pollutant diffusion in a forest canopy flow occurs because of molecular diffusion, turbulent diffusion and sedimentation. The immediate turbulent effects in canopy flow occur in convection and turbulent diffusion. The study of canopy flow inside turbulence starts with in site experimentation, then wind tunnel experimentation, and with those two, numerical simulation. For this case, modified turbulence models and large eddy simulation are used. The modeling of this kind of turbulent flow is inserted in a perspective of the advanced closing of statistical turbulent moments in averaged fluid mechanics governing equations, and the use of the this models to simulate real and complex situation have to be associated to the properly numerical implementations. In a first look, the use of cylinders to represent a canopy is a vague analogy. But for a first approach and for representation of the drag effects of the air-canopy interaction, a cylinder matrix will suffice (Seginer et al., 1976).

Inhomogeneous canopy flow problems gained major impulse at the nineties (Lee, 2000). Some of those studies include, for instance, flows through cutblocks (Wilson and Flesch, 1999) or over complex forested reliefs (Kobayashi et al., 1994, Ross et al., 2004). For this kind of problem, advanced turbulence models considering the vegetative canopy layers have been proposed. A real complex flow through and over forested reliefs occurs in a domain with a bottom surface issued from the topography of geographic regional terrain database. Sometimes, great gradients of elevation are encountered, and over this relief the vegetation is often distributed non-uniformly, due to different structures of the vegetative layer and to the existence of clearings. The study of Miguel et al., 2001 show a approach for the analysis of the airflow in closed spaces. On the developing the momentum equation with volume averaging, the author obtained a differential equation that can be numerically resolved. That equation was resolved with a unidimensional approach. Its results shown great agreement with experimental data. The PhD. thesis of Patton, 1997 presents a modified version of large eddy simulation to include aerodynamic and thermodynamic effects of canopy elements. The main objective is study the interaction of those canopy elements with the atmospheric boundary layer. The results show a slowdown in the turbulence redeveloping. The results of turbulent kinetic energy, average and fluctuation show good agreement with experimentation and field measures. Novak et al., 2000 studied, with wind tunnel experimentation, small scale models and direct measurement at the forest for canopy flows in Scotland. All the results obtained show the same patterns of canopy flow, and when those results were compared, those patterns became more clear. The work of Lai et al., 2000 discusses the creation of a complete Eulerian-Lagrangean model to study small weather effects in canopy flows. The main objective is to investigate CO<sub>2</sub> exchange rates between the forest and the airflow. The quantities studied were momentum, heat and mass flux, and radiation heat flux. The results for those fluxes were considered as good by the authors. Fitzmaurice et al., 2004 used large eddy simulation for a canopy flow to study micro-sources of flow quantities. Several numerical measures show similar pattern to experimental measurements and other numerical analysis. The work of Seginer et al., 1976 is a wind tunnel experiment at a cylinder matrix. The three component of the averaged velocity and its fluctuations are measured using a hot wire anemometer. The experiments were over a matrix covered by a barrier and without the barrier. The results obtained for both situations show that a small part of the turbulence inside the matrix has its origin at the

individual wake of the canopy elements. The average velocity is adjusted to the exponential profile. A experimental study of a small forest model based on a single cylinder and a cylinder matrix (Cala, 1996) in wind tunnel obtained profiles who had shown great resemblance with similar work.

The present work will analyze the results obtained by Noieto, 2006 by using the spatial averaging of Raupach and Shaw, 1982. The spatial average of the velocity will be calculated, alongside with its fluctuation. Then, a dispersive percentage will be calculated and displayed in contour format pictures, in order to identify how far from the average the local flow is.

## 2. MATHEMATICAL FORMULATION

### 2.1 Governing Equations

In a frame work for turbulence modeling, for incompressible turbulent flows, the conservation of mass, and momentum can be expressed by the classical Reynolds averaged equations given by:

$$\frac{\partial u_i}{\partial x_i} = 0 \quad (1)$$

$$\rho \frac{\partial u_i}{\partial t} + u_j \frac{\partial u_i}{\partial x_j} = -\frac{1}{\rho} \frac{\partial p}{\partial x_i} + \frac{\partial}{\partial x_i} \left[ (\nu + \nu_t) \left( \frac{\partial u_i}{\partial x_j} + \frac{\partial u_j}{\partial x_i} \right) \right] \quad (2)$$

In those equations  $u_i$  and  $p$  are the mean velocity and pressure fields.

### 2.2 The SST Model

Menter (Menter et al., 2003) created the SST model, and its principle lies on blending the  $k - \varepsilon$  and the  $k - \omega$  model. Far from the wall, the model uses the  $k - \varepsilon$  formulation, and near the wall, the model uses the  $k - \omega$  model. The transport equations are:

$$\rho \left( \frac{\partial k}{\partial t} + u_i \frac{\partial k}{\partial x_i} \right) = P_k - \beta' k \omega \rho + \frac{\partial}{\partial x_i} \left[ \left( \mu + \frac{\mu_t}{\sigma_k} \right) \frac{\partial k}{\partial x_i} \right] \quad (3)$$

$$\rho \left( \frac{\partial \omega}{\partial t} + u_i \frac{\partial \omega}{\partial x_i} \right) = \alpha \rho S^2 + \beta \rho \omega + \frac{\partial}{\partial x_i} \left[ \left( \mu + \frac{\mu_t}{\sigma_\omega} \right) \frac{\partial \omega}{\partial x_i} \right] + 2(1 - F_1) \rho \sigma_{\omega 2} + \frac{1}{\omega} \frac{\partial k}{\partial x_i} \frac{\partial \omega}{\partial x_i} \quad (4)$$

The eddy viscosity is defined by:

$$\nu_t = \frac{\alpha_1 k}{\max(\alpha_1 \omega, (S_{ij} S_{ij})^{\frac{1}{2}} F_2)} \quad (5)$$

$S$  is an invariant measure of the tensor rate and  $F_2$  is one of two blending functions of the model. The formulation of the blending functions  $F_1$  and  $F_2$  are based on the distance from the surface and on the flow's variables. The blending functions  $F_1$  and  $F_2$  are given as follows:

$$F_1 = \tanh(\arg_1^4) \quad (6)$$

$$\arg_1 = \min \left[ \max \left( \frac{\sqrt{k}}{\beta' \omega}, \frac{500\nu}{y^2 \omega} \right), \frac{4\rho \sigma_{\omega 2} k}{CD_{k\omega} y^2} \right] \quad (7)$$

$$CD_{k\omega} = \max(2\rho \sigma_{\omega 2} \frac{1}{\omega} \nabla k \nabla \omega, 1, 0.10^{-10}) \quad (8)$$

Here,  $y$  is the distance to the wall.  $F_1$  is equal to zero away from the surface ( $k - \varepsilon$ ), and switch over to 1 inside the boundary layer ( $k - \omega$  model).  $F_2$  is given by:

$$F_2 = \tanh(\arg_2^2) \quad (9)$$

$$\arg_2 = \max \left( \frac{2\sqrt{k}}{\beta' \omega y}, \frac{500\nu}{y^2 \omega} \right) \quad (10)$$

$F_2$  restrains the limiter for the boundary layer wall. A production limiter is used to avoid the growth of turbulence in stagnation regions:

$$P_k = \mu_t \frac{\partial U_i}{\partial x_j} \left( \frac{\partial U_i}{\partial x_j} + \frac{\partial U_j}{\partial x_i} \right) \quad (11)$$

$$\widetilde{P}_k = \max(P_k, 10 \cdot \rho \beta^* k \omega) \quad (12)$$

The model's constants are accounted by a blend of the corresponding constants of the  $k - \varepsilon$  and  $k - \omega$  models with the following function:

$$\alpha = \alpha_1 F_1 + \alpha_2 (1 - F_1) + \dots \quad (13)$$

The constants are  $\beta = 0.09$ ,  $\alpha_1 = 5/9$ ,  $\beta_1 = 3/40$ ,  $\alpha_{k1} = 0.5$ ,  $\sigma_1 = 0.5$ ,  $\alpha_2 = 0.44$ ,  $\beta_2 = 0.0828$ ,  $\sigma_{k2} = 1$ ,  $\sigma_2 = 0.856$ . The analytical expression for  $\omega$  provided by  $\omega$ -equation turbulence models allows a near-wall formulation, which gradually switches from wall-functions to low-Re near wall formulations. At the same time, the mesh is refined in wall normal direction.

### 2.3 Averaging Formalism

The modeling of canopy turbulent flows considers a *rationale* based in a double averaging process: In a first step all flow quantities are averaged on time using a characteristic time interval, like for free turbulent flows (this averaging operator is denoted by a overline bar symbol  $\overline{(\cdot)}$ ). In the second step a spatial averaging is performed within a reference volume (this operator is denoted by a bracket symbol  $\langle (\cdot) \rangle$ ). Discussions of the use and necessity of this formalism are developed in Raupach and Shaw, 1982 or Finnigan, 2000, for instance. The assumptions of incompressibility of the air flow under neutrally buoyancy conditions and no-waving behavior of canopy elements, were considered. Knowing that the numerical results obtained were averaged by the total time (this averaging is inherent to the URANS approach), the axial velocity ( $u$ ) results were submitted to a specific horizontal spatial averaging within a referenced area. This area is a symmetry plane taken at the far downstream of the cylinder matrix, where the flow has a boundary layer pattern. The flow over the matrix is three-dimensional by nature. The role played by this averaging is to allow the study of 3-D flows by a 1-D approach. Therefore effects like form and viscous drag, emission or absorption of turbulent wakes can be analyzed by the averaging process. The horizontal average operator present in Raupach and Shaw, 1982 to canopy flows will be used. For a given field of the flow, and excluding the points inserted in solid surfaces, the formal definition of horizontal average is given as follows:

$$\langle u \rangle = \frac{1}{A} \int \int_{\Psi} u(x) dx dy \quad (14)$$

This average is taken in all the area represented by the  $\Psi$  region. This region is multiply connected because of the intersection of the region with the canopy elements (The cylinders, for the present work). This operator satisfies all the properties of a averaging operator, excepting the commutative property in certain situations. Let  $C$  the contour of the region  $\Psi$ , as seen at figure 1. This contour does not intersect with any element of the matrix. The internal contours  $C_i$  inside the region define the interface between the flow and the canopy elements. If  $u$  is constant at those interfaces, than the horizontal average and its spatial derivatives can commute by the following (For  $i=1,2$ ):

$$\left\langle \frac{\partial u}{\partial x_i} \right\rangle = \frac{\partial \langle u \rangle}{\partial x_i} \quad (15)$$

From the base cylinder, 8 horizontal positions were considered in order to observe the fluctuation of the flow (figure 2). This analysis has the aim of a threshold of the flow, in order to pinpoint adequate locations for anemometer positioning, and velocity measuring. After the calculation of the spatial averaged velocity,  $\bar{u}$ , equation 16 were applied in order to obtain the spatial fluctuation:

$$u' = u - \langle u \rangle \quad (16)$$

After that, a dispersive percentage ( $dp(u)$ ) were calculated and plotted upon the horizontal planes. This percentage is calculated by equation 17:

$$dp(u) = \frac{|\langle u \rangle - u'|}{\langle u \rangle} \quad (17)$$

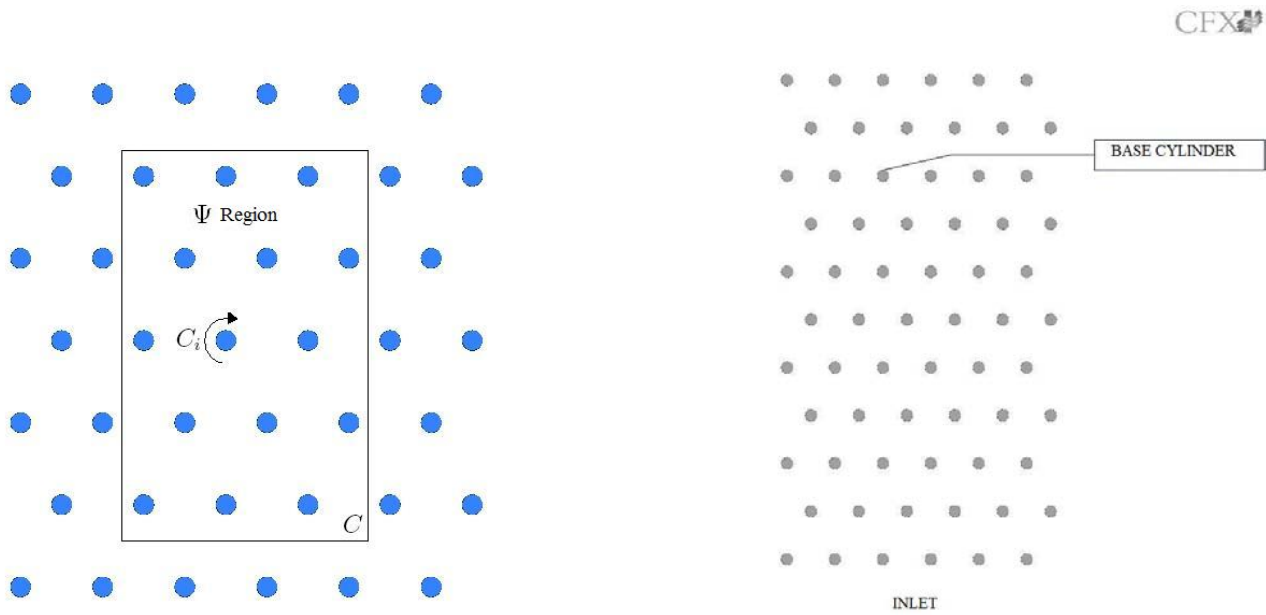


Figura 1.  $\Psi$  Region and cylinder base

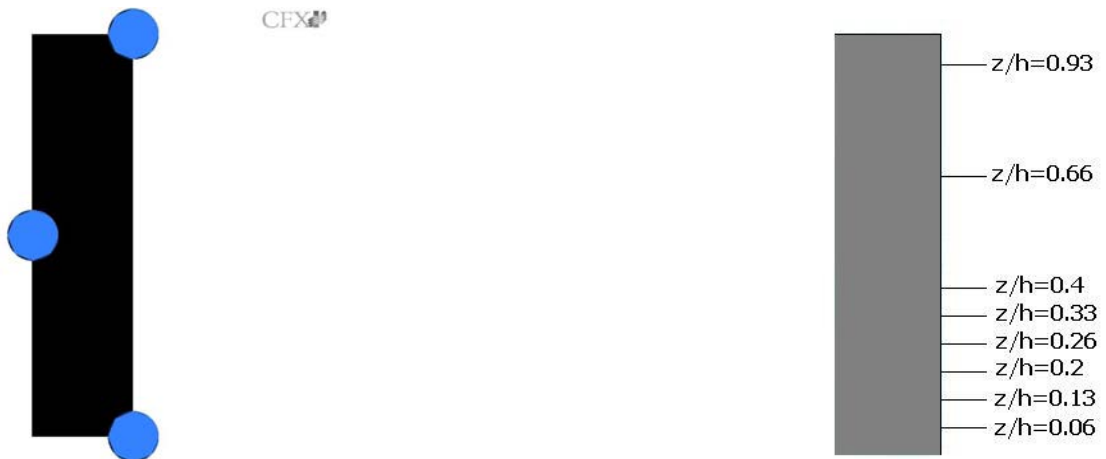


Figura 2. Symmetry plane display and positions

### 3. COMPUTATIONAL DETAILS AND BOUNDARY CONDITIONS

For inflow surfaces the values of velocity, kinetic energy of turbulence and dissipation fields are prescribed. For outflow boundaries, the homogeneous Neumann conditions are prescribed for the same variables and the homogeneous Dirichlet boundary condition is used for the pressure field. At the inlet, the following profile was imposed. This profile was measured by Cala et al., 1996 and approximated by an exponential function:

$$\frac{u}{u_0} = 1,089 \left( \frac{z}{H} \right)^{\frac{1}{6}} \quad (18)$$

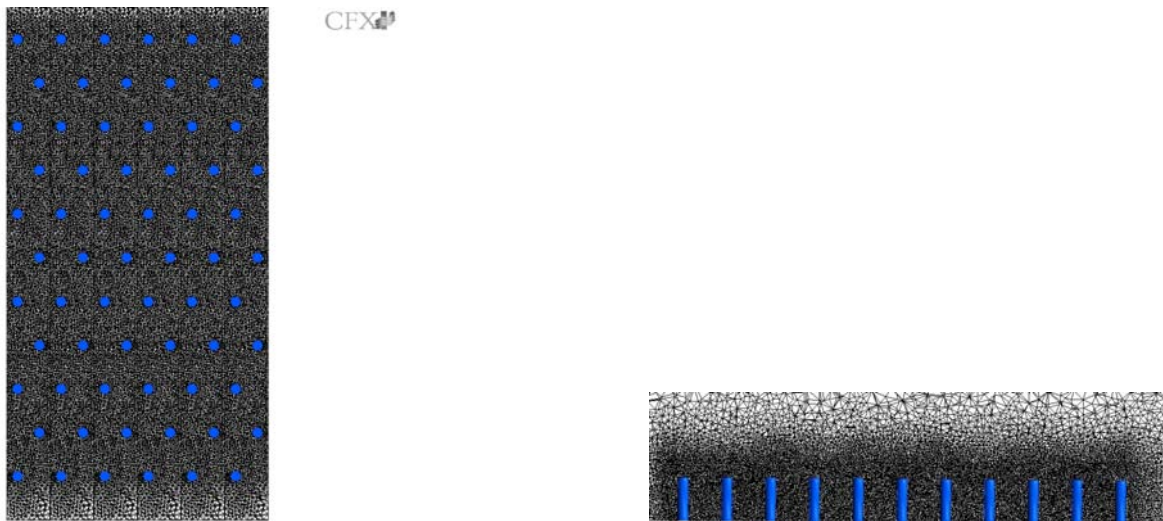


Figura 3. Grid display

The matrix studied by Cala, 1996 is a matrix array of 88 cylinders in tandem arrangement, without pendulum movement, attached to the lower wall. For this case, experimental results of transversal and vertical velocity, respective fluctuations and turbulent intensity are available. Each cylinder has 75 mm of height and diameter of 19 mm. The inlet Reynolds number based on the diameter of the cylinder is set by the velocity profile to the valor of 21000. Figure 3 shows the unstructured mesh used. There is a refinement at the surroundings of the cylinder and downstream of the domain. Here, the mesh has 185420 nodes and 1034325 elements. The transient simulation has a time step of  $10^{-3}$  seconds with a total time of 100 seconds. The convergence criterion is set as  $10^{-4}$  in RMS value of all fields norm.

#### 4. RESULTS

Figure 4 shows the numerical results of the matrix. The velocity isosurfaces and 3-dimensional streamlines shows the resemblance of the flow with the basic boundary layer flow. The canopy flow problem in forests and cities is basically a boundary layer problem. The boundary layer contains the canopy elements. The velocity isosurface shows that the smaller velocities are present at all the extensions of the matrix, and the higher velocities are present only at the upstream part of the matrix. At the third and fourth row of cylinders, the isosurfaces of higher velocities begin to ascend, configuring a typical visualization of a boundary layer in a flat plate. The increase of velocity not only denote the boundary layer pattern, but also shows a part of the interaction between the boundary layer and the free airflow. The 3-dimensional streamlines show that inside the matrix, the flow is completely turbulent due to the influence of the canopy elements. At this region, some flow phenomena, like drag, momentum transport, and depending of the case, mass and thermal transport is maximized. Figure 4 shows also a upper view of the matrix. The velocity contours close to the flat plate make evident the turbulent wake generated by the matrix. There is the occurrence of Von Kármán vortex formation. The formation of some coherent structures at the upstream rows of the matrix influences the wake of the downstream rows. At the sixth row, the wake becomes close to symmetry. But, at downstream rows, the Von Kármán wake happens again. That wake is responsible for the conversion of average kinetic energy in turbulent kinetic energy, at the characteristic scale of the canopy elements.

Figure 5 shows the velocity and turbulence intensity for the matrix, at a distance of four diameters from the cylinder base. Those results were plotted with the experimental results of Cala, 1996. The turbulence intensity was calculated with the turbulent kinetic energy. To the Reynolds number of the flow, a slight decay of the velocity is observed. To overcome drag effects, a high amount of kinetic energy is needed, and this can inhibit any ascending flow. The graphic shows that the velocity is constant and smaller when compared with the free stream flow, due to the fact that the velocity reduces inside the matrix. At  $2/3$  of the height of the matrix, the velocity increases. This shows that the upstream effects at the top affect the flow, as seen in Seginer et al., 1976. The numerical result also shows the inflexion noted at the experimental results. The turbulence intensity profiles show a peak at its values. This is a evidence of the flow perturbation caused by top effects of the cylinders.

The figures 6, 7, 8 and 9 has a scale from 0 to 1. The dispersive percentage is a indicative of how the fluctuations are away from the averaged flow. Therefore, it can indicate adequate places for flow probes. At  $z/h = 0.06$ , there are occurrences of red zones at the wake of the cylinders. The middle cylinder has most of it all occurrences, which indicates that the cylinder wakes concentrate all the canopy turbulence. This vertical position holds great difficulty in velocity measurement by anemometry due to the fact that its position is very close to the canopy ground. This happens because of the occurrence of several turbulent phenomena, like horseshoe vortex. In fact, the vortex shedding observed at figure

4 happens at this location. The green and blue zones happens at upstream and at the middle of the symmetry plane. Those zones indicates a good measurement position. A important point to be highlighted is that the wake of one cylinder affects the flow of the cylinders downstream of it. The blue zones are an effect of this influence. For horizontal planes  $z/h = 0.13, z/h = 0.2, z/h = 0.26, z/h = 0.33, z/h = 0.4, z/h = 0.66$ , the red zones at the wake also happens, but this zones are slowly diminished when the height increases. This indicates that the canopy turbulence within the matrix has a typical boundary layer behavior, with high variations of flow quantities at a short range of height. It is also confirms that the turbulence of this kind of problem is mainly concentrated at regions close to the ground. The blue and green zones also shows increase with the height increase. This is also a indicative of the boundary layer behavior within the matrix. At  $z/h = 0.93$  the red zones disappeared, with occurrence of green zones at the middle of the symmetry plane. This is a signal of the free end wake flow. From  $z/h = 0.66$  to  $z/h = 0.93$ , the dispersive display suffered major difference. This is caused also by the free end wake flow. This kind of flow, common in flow across finite cylinders, can be characterized by necklace vortex (if the aspect ratio is high) or small structures that become bigger when the height decreases (if the aspect ratio is small). The  $z/h = 0.93$  horizontal plane shows blue zones at the cylinders wakes. That is a indication of the non-existence or occurring of small turbulent structures at the free end of the cylinder. Based on all results, it can be inferred that, after a thorough threshold of the planes, the good positions of flow measurement are places that are outside of wakes or any turbulent structures. So, the blue zones indicates the best measuring positions. Those zones are places where are no concentration of turbulence at the canopy. Therefore, the measures will not be tainted by extreme vorticity or intense fluctuations. But, with advanced measurement techniques, like particle imaging velocimetry or laser induced fluorescence, those zones can be easily identified and measured.

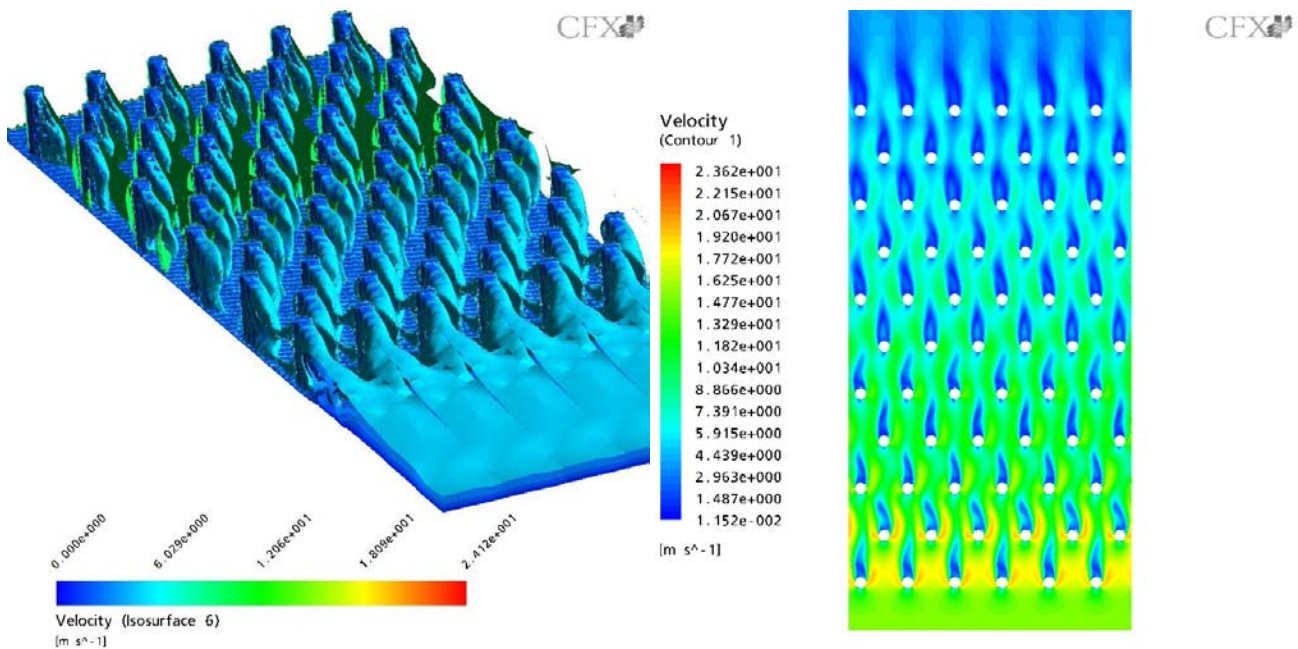


Figura 4. Flow Visualization

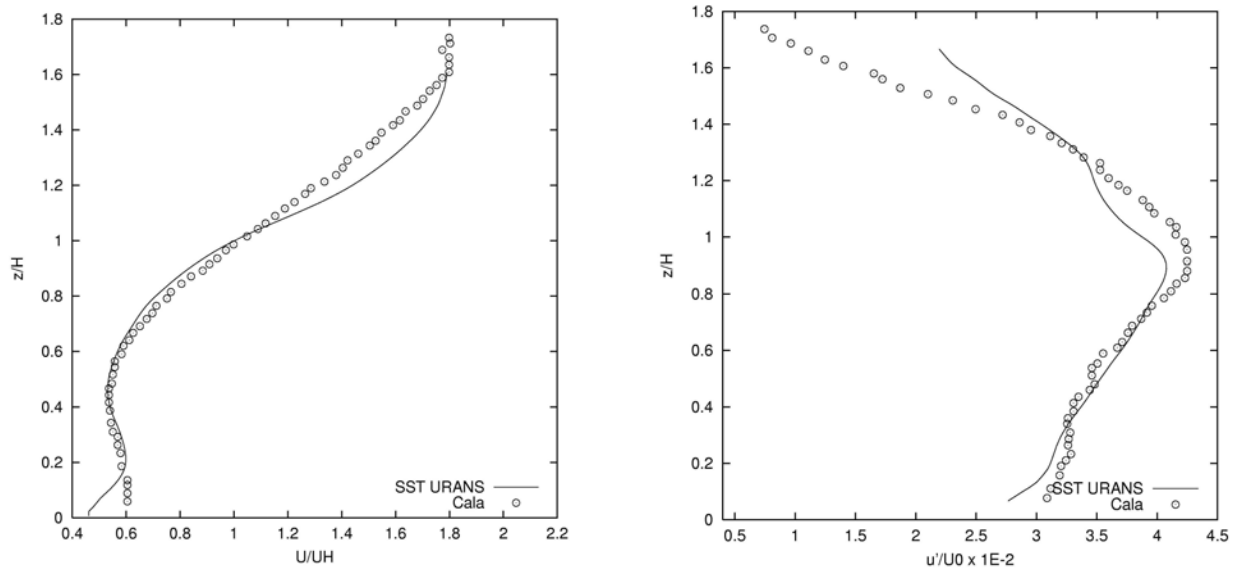


Figure 5. Velocity and Turbulent Intensity Profiles taken from the wake of the cylinder base

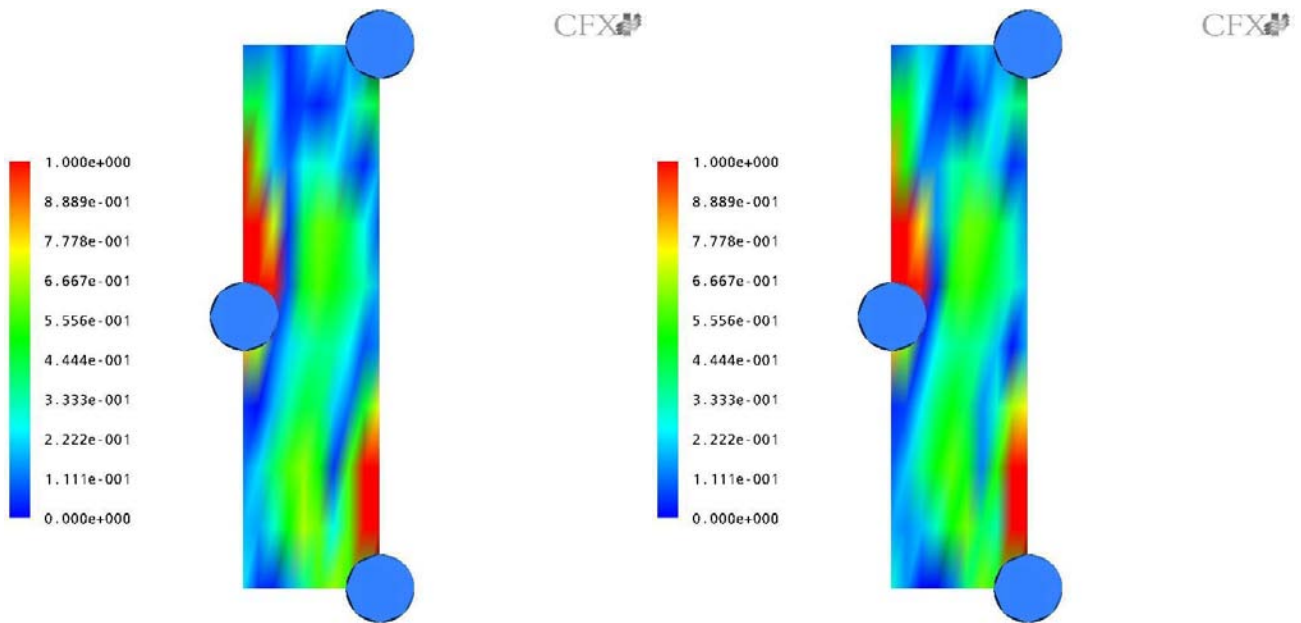


Figure 6. Dispersive Percentage - From left to right -  $z/h = 0.06$  and  $z/h = 0.13$

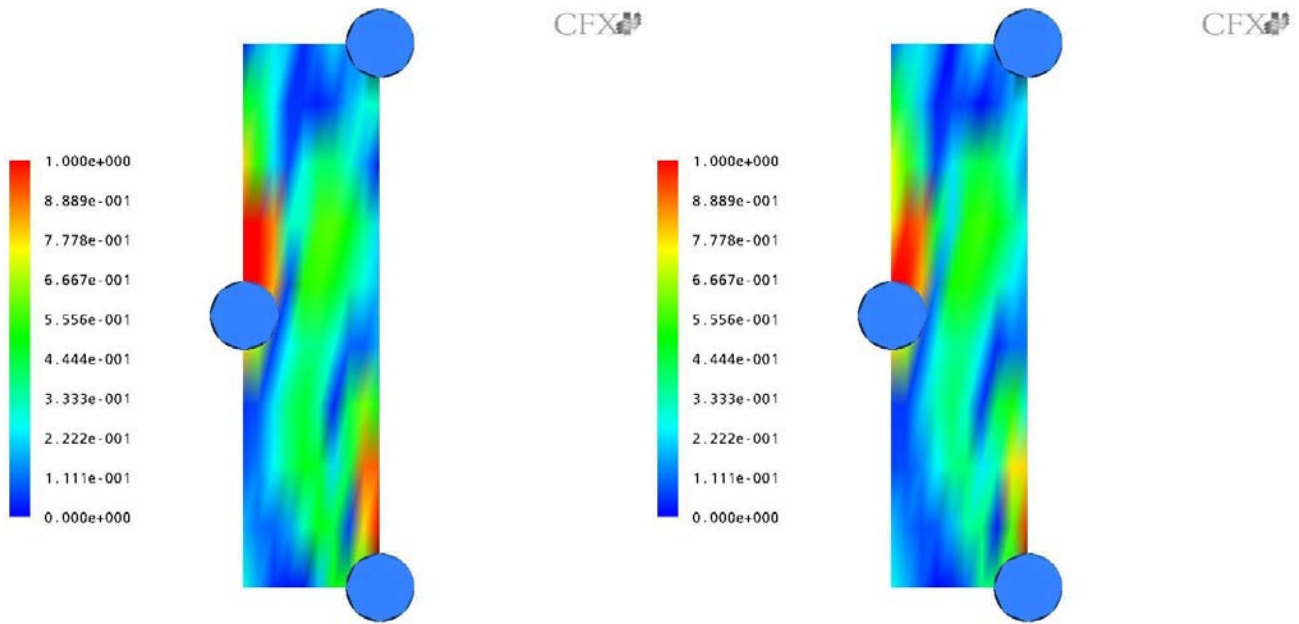


Figura 7. Dispersive Percentage - From left to right -  $z/h = 0.2$  and  $z/h = 0.26$

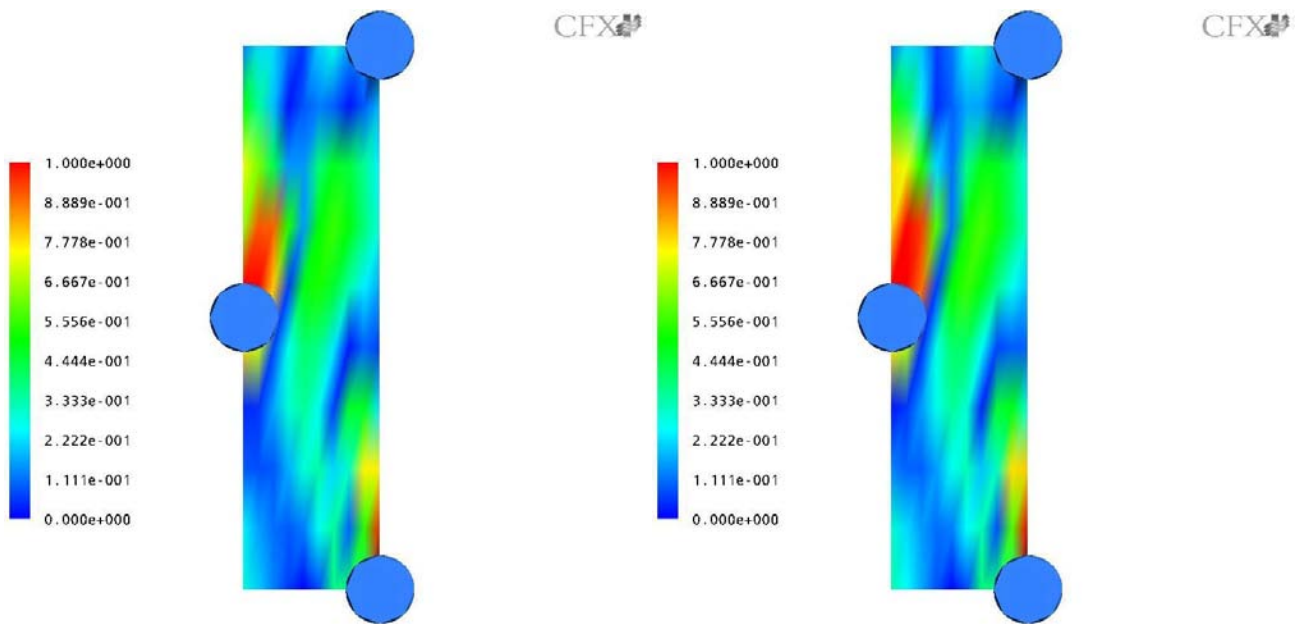


Figura 8. Dispersive Percentage - From left to right -  $z/h = 0.33$  and  $z/h = 0.4$

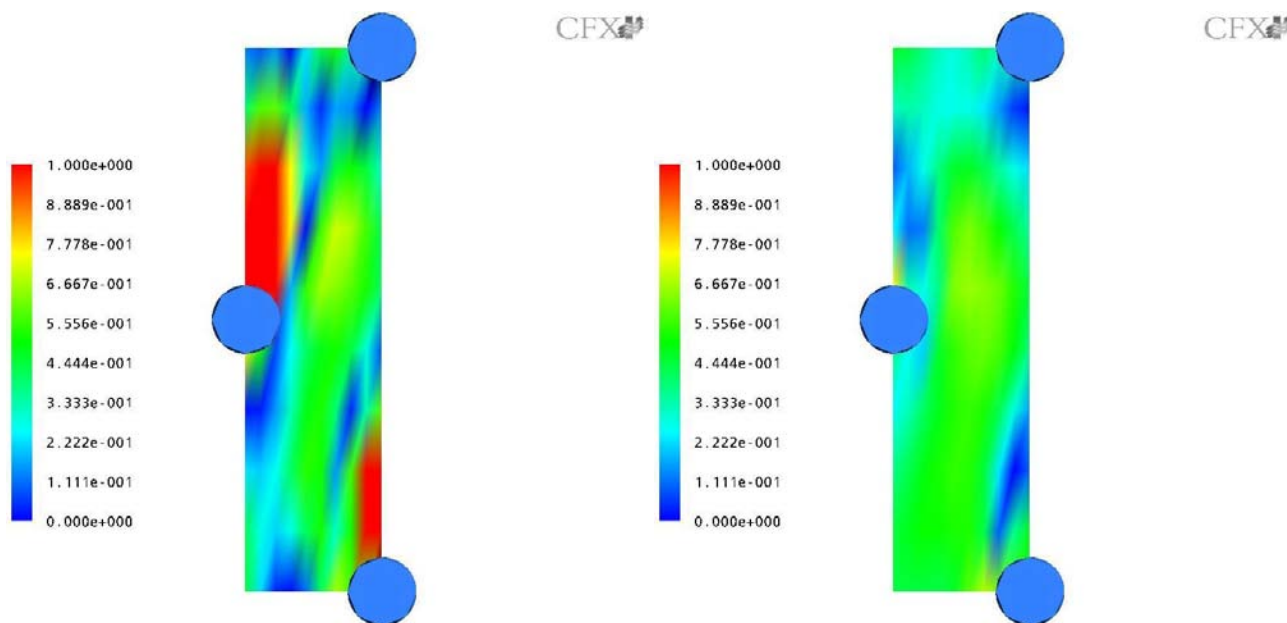


Figura 9. Dispersive Percentage - From left to right -  $z/h = 0.66$  and  $z/h = 0.93$

## 5. CONCLUSION

Results of a numerical simulation over a cylinder matrix to approach a canopy flow were presented. The showed results include velocity vectors, streamlines, velocity isosurfaces, velocity and turbulent intensity profiles and a averaging analysis.

The visualization results of the numerical simulation shows the typical boundary layer pattern of this kind of flow. The side visualizations show the thickening of the boundary layer over the flat plate. They also show how the matrix and the boundary layer interact. There are also visualizations of vortex shedding at the matrix, and the interaction of the downstream cylinders on the wake. The experimental results are shown in velocity profiles taken downstream of a base cylinder. Those results show the increase of the velocity close to the free end of the cylinders, which agree with similar work. The averaging results shows that, for several heights, there are zones where velocity measurement will not produce good results. At those zones, the spatial fluctuation is apart from the average, as shown by the dispersive percentage. Those zones are placed at the wake of the cylinders and more intense close to the ground. This is an effect of the near wall effects, like the horseshoe vortex. The more far from the ground the plane is, the less intense the red zones become. At the highest symmetry plane, the red zones disappeared. At that place, the average flow is close to its fluctuation. Zones where are good to place flow probes are located at the blue zone showed at the figures.

Concluding, the results showed by the present work can be considered as good, as the averaging discussion. For the future, it is considered for this case the simulation with large eddy simulation and detached eddy simulation. Also, an analysis of the dispersive percentage above the cylinder matrix, far from the boundary layer, can be useful for studying the flow.

## 6. REFERENCES

- Cala, C. E. C., 1996, Estudo do Escoamento Turbulento Dentro e Sobre uma Matriz de Cilindros Pendulares, Master's thesis, Universidade de Brasília, DM-018.
- Cala, C., Brasil-Junior, A. C. P., e Sousa, A. J. (1996). Escoamento Turbulento em Torno de um Cilindro Pendular. Proceedings of VI ENCIT - The Brazilian Congress of Thermal Engineering and Sciences.
- Finnigan, J. J., 2000, Turbulence in plant canopies, "Annual Review of Fluid Mechanics", Vol. 32, pp. 519-571.
- Fitzmaurice, L., Shaw, R. H., Pwau, K. T., and Patton, E. G., 2004, 3-Dimensional Scalar Microfront Systems in a Large Eddy Simulation of Vegetation Canopy Flow, "Boundary Layer Metereology", Vol. 112, pp. 107-127.
- Kobayashi, M., Pereira, J., and Siqueira, M., 1994, Numerical Study of the Turbulent Flow over and in a Model Forest on a 2D Hill, "J. Wind Eng. Ind. Aerodyn.", Vol. 53, pp. 357-374.
- Lai, C. T., Katul, G., Ellsworth, D., and Oren, R., 2000, Modelling Vegetation- Atmosphere CO2 Exchange by a Coupled Eulerian-Lagrangean Approach, "Boundary Layer Metereology", Vol. 95, pp. 91-122.
- Lee, X., 2000, Air motion within and above forest vegetation in non-ideal conditions, "Forest Ecology and Manage-

ment”, Vol. 135, pp. 2–18.

Menter, F. R., Kuntz, M., and Langtry, R., 2003, Ten years of industrial experience with the SST turbulence model, “Turbulence, heat and Mass transfer”, Vol. 4.

Miguel, A., de Braak, N., Silva, A., and Bot, G., 2001, Wind-induced air flow through permeable materials, “Journal of Wind Engineering and Industrial Aerodynamics”, Vol. 89, pp. 45–57.

Noleto, L. G., 2006, Estudo Numérico do Escoamento Turbulento em Modelos Florestais, Master’s thesis, Universidade de Brasília, DM-103.

Novak, M. D., Warland, J. S., Orchansky, A. L., Ketler, R., and Green, S., 2000, Wind Tunnel and Field Measurements of Turbulent Flow in Forests part 1: Uniformly thinned Stands, “Boundary Layer Meteorology”, Vol. 95, pp. 457–495.

Patton, E. G., 1997, “Large Eddy Simulation of Turbulent Flow Above and Within a Plant Canopy”, PhD thesis, University of California.

Raupach, M. R. and Shaw, R., 1982, Averaging Procedures for Flow Within Vegetation Canopies, “Boundary-Layer Meteorology”, Vol. 2, pp. 427–459.

Ross, A., Arnold, S., Vosper, S., Mobbs, S., Dixon, N., and Robi, A., 2004, A Comparison of wind tunnel experiments and numerical simulations of neutral and stratified flow over a hill, “Boundary-Layer Meteorology”, Vol. 113, pp. 427–459.

Seginer, I., Mulhearn, P. J., Bradley, E. F., and Finnigan, J. J., 1976, Turbulent flow in a model plant canopy, “Boundary Layer Meteorology”, Vol. 10, pp. 423 – 453.

Wilson, J. and Flesch, T., 1999, Wind and remnant tree sway in forest cutblocks. III. a wind flow model to diagnose spatial variations, “Agricultural and Forest Meteorology”, Vol. 93, pp. 259–282.